Human *RAP2A* Homolog of the *Drosophila* Asymmetric Cell Division Regulator *Rap2l* Targets the Stemness of Glioblastoma Stem Cells

Maribel Franco[1], Ricardo Gargini[2], Víctor M. Barberá[3, 4], Miguel Saceda[4] and Ana Carmena[1*]

[1]Instituto de Neurociencias, Consejo Superior de Investigaciones Científicas/Universidad Miguel Hernández de Elche, Sant Joan d'Alacant 03550, Alicante, Spain

[2]Instituto de Investigación Biomédicas I+12 and Pathology and Neurooncology Unit, Hospital Universitario 12 de Octubre, Madrid 28041, Spain

[3]Unidad de Genética Molecular, Hospital General Universitario de Elche, Camí del'Almazara 11, Elche, 03203, Alicante, Spain

[4]Unidad de Investigación, Fundación para el Fomento de la Investigación Sanitaria y Biomédica de la Comunidad Valenciana (FISABIO), Hospital General Universitario de Elche, Camí del'Almazara 11, Elche, 03203, Alicante, Spain

Running title: Human RAP2A Targets the Stemness of GSCs

***Corresponding author:** acarmena@umh.es; Instituto de Neurociencias, Consejo Superior de Investigaciones Científicas/Universidad Miguel Hernández de Elche, 03550-Sant Joan d'Alacant, Alicante, Spain

Abstract

Asymmetric cell division (ACD) is a fundamental process to balance cell proliferation and differentiation during development and in the adult. Cancer stem cells (CSCs), a very small but highly malignant population within many human tumors, are able to provide differentiated progeny by ACD that contribute to the intratumoral heterogeneity, as well as to proliferate without control by symmetric, self-renewing divisions. Thus, ACD dysregulation in CSCs could trigger cancer progression. Here we consistently find low expression levels of *RAP2A*, the human homolog of the *Drosophila* ACD regulator *Rap2l*, in glioblastoma (GBM) patient samples, and observe that scarce levels of *RAP2A* are associated with poor clinical prognosis in GBM. Additionally, we show that restitution of RAP2A in GBM neurosphere cultures increases the ACD of glioblastoma stem cells (GSCs), decreasing their proliferation and expression of stem cell markers. Our results support that ACD failures in GSCs increases their spread, and that ACD amendment could contribute to reduce the expansion of GBM.

49 **Introduction**

50 Asymmetric cell division (ACD) is a universal mechanism for generating cellular
51 diversity during development as well as for regulating tissue homeostasis in the adult
52 (1). Stem and progenitor cells undergo ACD to simultaneously give rise to a self-
53 renewing stem/progenitor cell and to a daughter cell that is committed to enter a
54 differentiation program. Remarkably, over the past years it has become apparent that
55 undermining this critical process can lead to tumor-like overgrowth (2). This link
56 between failures in the process of ACD and tumorigenesis was first established using
57 the *Drosophila* neural stem cells, called neuroblasts (NBs), as a model system (3). In
58 this work, authors showed how *Drosophila* larval mutant brains for ACD regulatory
59 genes were able to induce the formation of massive tumoral masses after weeks of
60 being transplanted into the abdomen of wild-type fly hosts. Intriguingly, some genes
61 firstly identified in *Drosophila* as tumor suppressor genes, such as *discs large 1* (*dlg1*),
62 *lethal (2) giant larvae* (*l(2)gl*) and *brain tumor* (*brat*) (4), were later uncovered as ACD
63 regulators (5-11), further supporting the connection between compromised ACD and
64 tumorigenesis.

65 Tumor initiating cells or cancer stem cells (CSCs) were originally identified in
66 acute myeloid leukemia (AML) (12,13) but, to date, several studies have also revealed
67 the existence of CSCs in multiple solid tumors (14). These CSCs represent a very small
68 but highly malignant population within the tumor, able to proliferate without control
69 by symmetrical, self-renewal divisions, as well as to provide differentiated progeny by
70 ACD that contribute to the heterogeneity of the tumor. These properties, along with
71 their quiescent state, increase in metabolic activity and high capacity of DNA repair,
72 make CSCs extremely resistant to radio- and chemotherapy and responsible for

73 malignant relapse (14-18). Thus, understanding the unique nature of these cells and
74 their landmarks is crucial to target CSCs and hence to completely destroy the tumor.
75 An intriguing possibility is that an unbalanced ACD process in CSCs, favoring symmetric
76 renewal divisions, might contribute to the transition from a chronic (low grade) to an
77 acute (high grade) phase in the cancer progression (19,20).

78 Glioblastoma (GBM), the most aggressive and lethal brain tumor with very poor
79 prognosis, is among the solid tumors in which the presence of CSCs, called glioma or
80 glioblastoma stem cells (GSCs), has been proven. As other CSCs, GSCs are responsible
81 for the formation, maintenance, resistance to conventional therapy and consequent
82 relapse of GBM (21-25). Several GSC biomarkers, such as CD133 and Nestin, and
83 signaling pathways, such as Notch and Hedgehog, have been identified to help isolate
84 and target these crucial cells (14,26,27). Despite of that, there are still many unknowns
85 regarding the nature, properties and origin of CSCs in general and of GSCs in particular.

86 Here, we analyze the consequences of compromising ACD in the GSCs within
87 GBM neurosphere cell cultures. Specifically, we show that *RAP2A*, the human homolog
88 of *Rap2l*, which encodes a *Drosophila* small GTPase and novel ACD regulator, displays
89 low expression levels in GBM, and that restitution of RAP2A in GBM neurosphere
90 cultures increases the ACD and decreases the expression of stem cell markers in the
91 GSCs. Our results support that failures in ACD increase GSC proliferation promoting
92 their spreading and that ACD amendment might contribute to reduce the expansion of
93 GBM.

94

95

96

97 **Results**

98 **RAP2A is highly downregulated in GBM patients**

99 As a first approach to analyze whether ACD might be impaired in GBM, we analyzed
100 the expression levels of human homologs of 21 *Drosophila* ACD regulators in a GBM
101 microarray (28) (Fig. 1A). We also investigated which of those genes were more similar
102 in expression pattern to the others by performing a Gene Distance Matrix (**Fig. 1B**).
103 The human genes *TRIM2* and *RAP2A* showed the lowest levels in the GBM patient
104 samples analyzed. *TRIM2* belongs to the same family that *TRIM3* and *TRIM32*, all of
105 them related to the *Drosophila* ACD regulator gene *brat*. *TRIM3,* the closest homolog
106 of *brat*, has been previously found to be expressed at low levels in GBM (29). Hence,
107 we concentrated on *RAP2A*, the second human gene consistently found at very low
108 levels in all the patient samples (**Fig. 1A**). *RAP2A* is also known to have a tumor
109 suppressor role in the context of glioma migration and invasion (30,31). First, to
110 further support the microarray data expression levels in a bigger sample size, we
111 performed *in silico* analyses taking advantage of established datasets of Glioblastoma
112 IDH wild-type, such as "The Cancer Genome Atlas" (TCGA) and “Gravendeel cohort”.
113 We confirmed that low *RAP2A* expression levels in human GBM are associated with a
114 poor prognosis (**Fig. 1C**). Hence, we focused on the human gene *RAP2A* to analyze its
115 potential role in ACD and its relevance in GBM.

116

117 ***Drosophila RAP2A* homolog *Rap2l* regulates ACD**

118 We previously showed that the *Drosophila* gene *Rap1* regulates the ACD process (32).
119 The closest human homolog of *Drosophila Rap1* is *RAP1A*, while human *RAP2A* is more
120 similar to *Drosophila Rap2l,* which has not been previously analyzed in the context of

121 ACD. Hence, we first wanted to investigate whether *Rap2l* was, like *Rap1*, implicated in
122 ACD regulation. With that aim, we started analyzing the ACD of neural stem cells
123 (neuroblasts, NBs) and intermediate neural progenitors (INPs) within *Drosophila* larval
124 brain type II NB lineages (NBII) (**Fig. 2A**) (8,33,34). In NBII lineages, there is one NB that
125 expresses the transcription factor Deadpan (Dpn) and several INPs, which express both
126 Dpn and the transcription factor Asense (Ase) (**Fig. 2A**). We first observed the presence
127 of ectopic NBs (eNBs; Dpn^+ Ase^-) after downregulating *Rap2l* in NBII lineages, while in
128 control lineages only one NB was usually found (**Fig. 2B**). This result suggested that the
129 process of ACD was impaired within those *Rap2l* mutant NBII lineages. To more
130 directly support that, we analyzed the localization of key ACD regulators in metaphase
131 NBs and INPs of NBII lineages, such as the apical proteins aPKC and Canoe (Cno), and
132 the cell-fate determinant Numb (35-37). In control metaphase NBs and INPs, those
133 ACD regulators form crescents at the apical (aPKC and Cno) or basal (Numb) poles of
134 the dividing cell (**Fig. 2C**). The apical localization of aPKC was not significantly altered
135 after downregulating *Rap2l* in NBII lineages; however, the localization of Cno and
136 Numb did fail (**Fig. 2C**). All these results strongly suggested that Rap2l, as Rap1, was an
137 ACD regulator. Hence, we came back to the human homolog of *Drosophila Rap2l*,
138 *RAP2A*, to determine its potential relevance in the context of the ACD of GSCs.
139

140 **RAP2A expression in GBM neurosphere cultures reduces the stem cell population**

141 After confirming by *in silico* analyses that low *RAP2A* expression levels in GBM patients
142 were associated to a poor prognosis, we decided to use established GBM cell lines to
143 investigate in neurosphere cell cultures whether the downregulation of *RAP2A* was
144 affecting the properties of GSCs. We tested six different GBM cell lines finding similar

145 mRNA levels of *RAP2A* in all of them, and significantly lower levels than in control
146 Astros (**Fig. 3A**). We focused on the GBM cell line called GB5, which grew well in
147 neurosphere cell culture conditions, for further analyses. Given that stem cell markers,
148 such as CD133, SOX2 and NESTIN are landmarks of GSCs, we started analyzing their
149 expression after restoring RAP2A in the neurosphere culture (**Fig. 3B**).
150 Immunofluorescences of each of those markers revealed a significant reduction in the
151 protein intensity in the RAP2A-expressing neurospheres (GB5-RAP2A) compared to the
152 control neurospheres (GB5) (**Fig. 3C**). Likewise, RT-PCRs and Westerns blots also
153 showed a significant decrease in the mRNA and protein expression levels, respectively,
154 of those stem cell markers (**Fig. 4**). Hence, RAP2A seems to be contributing to decrease
155 the stem cell population within GBM neurosphere cultures.
156
157 **RAP2A expression in GBM neurosphere cultures decreases cell proliferation and**
158 **sphere size**
159 Next, we wondered whether the reduction in the stem cell population after expressing
160 *RAP2A* in neurosphere cultures was reflected in the level of cell proliferation and,
161 consequently, in the size of the neurospheres. To investigate this, we first analyzed the
162 expression of the proliferation marker and key tool in cancer diagnostics Ki-67, highly
163 expressed in cycling cells but absent in quiescent (G0) cells (38,39). We detected a
164 significant decrease in the number of proliferating cells per neurosphere in those
165 cultures expressing *RAP2A* (**Fig. 5A**). Moreover, the average area size of these GB5-
166 RAP2A neurospheres was also significantly reduced compared to control GB5
167 neurospheres (**Fig. 5B**). Thus, RAP2A promotes a decrease in cell proliferation.
168

169 **RAP2A expression in GBM neurosphere cultures fosters ACD in GSCs**

170 Given the reduction in cell proliferation and in the stem cell population after adding
171 RAP2A to the control GB5 neurosphere cultures, we wanted to investigate whether
172 RAP2A was favoring an asymmetric mode of cell division in these cells. Thus, we
173 decided to follow over time the GB5-RAP2A and the control GB5 neurospheres,
174 analyzing the number of cells per neurosphere cluster. We reasoned that an even
175 number of cells per cluster would be indicative of symmetric cell divisions, while an
176 odd number of cells would point to an asymmetric mode of cell division. We observed
177 a significant increase of cell clusters with an odd number of cells in the GB5-RAP2A
178 neurospheres (n= 124 cell clusters analyzed) compared to control GB5 neurospheres
179 (n=153 cell clusters) (**Fig. 6A**). This result was very suggestive of an increase in the
180 number of ACDs in GB5-RAP2A neurosphere cells. To further support this result, we
181 decided to analyze the distribution of the cell fate determinant NUMB, a key
182 conserved ACD regulator whose asymmetric distribution in the mother and progeny
183 ultimately promotes the repression of stem cell self-renewal in the daughter cell in
184 which is segregated (40-44). We observed a significant increase in the number of GB5-
185 RAP2A dividing cells that showed an asymmetric localization of NUMB in the progeny,
186 compared to control GB5 dividing cells (**Fig. 6B**). Thus, all these results strongly
187 supported a function of RAP2A promoting ACD in the GSCs.

188

189

190

191

192

193 **Discussion**

194 ACD is an evolutionary conserved mechanism used by stem and progenitor cells to
195 generate cell diversity during development and to regulate tissue homeostasis in the
196 adult. CSCs, present in many human tumors, can divide asymmetrically to generate
197 intratumoral heterogeneity or symmetrically to expand the tumor by self-renewal.
198 Over the past 15 years, it has been suggested that dysregulation of the balance
199 between symmetric and asymmetric cell divisions in CSCs, favoring symmetric
200 divisions, can trigger tumor progression in different types of cancer (19,20,45)
201 including mammary tumors (43,46), glioblastoma (29), oligodendrogliomas (47,48),
202 colorectal cancer (49,50) and hepatocellular carcinoma (50). Thus, it is of great
203 relevance to get a deeper insight into the network of regulators that control ACD, as
204 well as the mechanisms by which they operate in this key process.

205 *Drosophila* neural stem cells or NBs have been used as a paradigm for many
206 decades to study ACD (51). NBs divide asymmetrically to give rise to another self-
207 renewing NB and a daughter cell that will start a differentiation process. Over all these
208 years, a complex network of ACD regulators that tightly modulate this process has
209 been characterized. For example, the so-called cell-fate determinants, including the
210 Notch inhibitor Numb, accumulate asymmetrically at the basal pole of mitotic NBs and
211 are exclusively segregated to one daughter cell, promoting in this cell a differentiation
212 process. The asymmetric distribution of cell-fate determinants in the NB is, in turn,
213 regulated by an intricate group of proteins asymmetrically located at the apical pole of
214 mitotic NBs, generically known as the "apical complex". This apical complex includes
215 kinases (i.e. aPKC), small GTPases (i.e. Cdc42, Rap1) and Par proteins (i.e. Par-6, Par3),
216 among others (51).

217 Given the potential relevance of ACD in CSCs, we decided to take advantage of
218 all the knowledge accumulated in *Drosophila* about the network of modulators that
219 control asymmetric NB division. As a first approach, we aimed to analyze whether the
220 levels of human homologs of known *Drosophila* ACD regulators were altered in human
221 tumors. Specifically, we centered on human GBM, as the presence of CSCs (GSCs) have
222 been shown in this tumor. The microarray we interrogated with GBM patient samples
223 had some limitations. For example, not all the human genes homologs of the
224 *Drosophila* ACD regulators were present (i.e. the human homologs of the determinant
225 Numb). Likewise, we only tested seven different GBM patient samples. Nevertheless,
226 the output from this analysis was enough to determine that most of the human genes
227 tested in the array presented altered levels of expression. We selected for further
228 analyses *RAP2A*, one of the human genes that showed the lowest levels of expression,
229 compared to the control samples. However, it would be interesting to analyze in the
230 future the potential consequences that altered levels of expression of the other human
231 homologs in the array can have in the behavior of the GSCs. In silico analyses, taking
232 advantage of the existence of established datasets, such as the TCGA, can help to more
233 robustly assess, in a bigger sample size, the relevance of those human genes
234 expression levels in GBM progression, as we observed for the gene *RAP2A*.

235 We have previously shown that *Drosophil*a Rap1 acts as a novel NB ACD
236 regulator in a complex with the apical regulators Canoe (Cno), aPKC and Par-6 (32).
237 Here we have shown that *Drosophila* Rap2l also regulates NB ACD by ensuring the
238 correct localization of the ACD modulators Cno and Numb. We also have
239 demonstrated that RAP2A, the human homolog of *Drosophila* Rap2l, behaves as an
240 ACD regulator in GBM neurosphere cultures, and its restitution to these GBM cultures,

241 in which is present at low levels, targets the stemness of GSCs increasing the number
242 of ACDs. Thus, this study supports the relevance of ACD in CSCs of human tumors to
243 refrain the expansion of the tumor. Other studies, however, claim that ACD should be
244 targeted in human tumors as it promotes the intratumoral heterogeneity that hampers
245 the complete tumor loss after chemotherapy (52-54). More studies should be carried
246 out with other human genes homologs of ACD regulators to further confirm the results
247 of this study. Likewise, analyses in vivo (i.e. in mouse xenografts) would be also
248 required to reinforce our conclusions. This would be very relevant in order to consider
249 ACD restitution in CSCs of human tumors, what has been called "differentiation
250 therapy" (55), as a potential alternative therapeutic treatment.
251
252
253

254 **Materials and Methods**

255 ***Drosophila* husbandry, strains and genetics**

256 The following fly stocks were used: *wor-Gal4 ase-Gal80 (56)*; *UAS-CD8::GFP*
257 (Bloomington *Drosophila* Stock Center -BDSC- #5137); *UAS-CD2* (BDSC #1373); *UAS-*
258 *Rap2l*^{KKRNAi} (Vienna *Drosophila* Resource Center #107745); *cno::GFP (57)*. All the fly
259 stocks were raised and kept in 18°C or 25°C incubators. Experimental temperatures for
260 the assays were maintained using 25°C or 29°C incubators. The *Gal-4* x *UAS*-crosses
261 were carried out at 29°C (the first 2 days they were kept at 25°C, and then transferred
262 to a new tube and left at 29°C) until third instar larvae developed.

263

264 ***Drosophila* histology, immunofluorescence and microscopy**

265 Larval brains were dissected out in PBS and fixed with 4% PFA in PBT (PBS and Triton X-
266 100 0.1%) for 20 min at room temperature with gentle rocking. Fixed brains were
267 washed 3 times for 15 min with PBT (PBS and Triton X-100 0.3%) and then incubated in
268 PBT-BSA for at least 1h before incubation with the corresponding primary
269 antibody/antibodies. The following primary antibodies were used in this study: guinea
270 pig anti-Dpn (1:2,000) (57), rabbit anti-Ase (1:100) (57), rabbit anti PKCζ (1:100; Santa
271 Cruz Biotechnology, sc-216), goat anti-Numb (1:200; Santa Cruz Biotechnology, sc-
272 23579), mouse anti-PH3 (1:2,000; Millipore, 05-806), mouse anti-γTub (1:200; Sigma-
273 Aldrich, T5326) and mouse anti-CD2 (1:50; BioRad). Secondary antibodies conjugated
274 to fluorescent dyes (Invitrogen) were used at 1:400 dilution. Samples were mounted in
275 VECTASHIELD antifade mounting medium for fluorescence (Vector Laboratories, H-
276 1000). Fluorescent images were captured using a Super-resolution Inverted Confocal

277 Microscope Zeiss LSM 880-Airyscan Elyra PS.1. Images were analyzed using the image
278 processing package FIJI from ImageJ and assembled using Adobe Photoshop CS6.
279
280 **GBM microarray**

281 The cohort of patients consisted of seven GBM biopsies obtained from the Valencian
282 Network of Biobanks. The procedures for obtaining tissue samples were developed in
283 accordance with national ethical and legal standards, and following the guidelines
284 established in the Declaration of Helsinki, and approved of Clinical Research Ethics
285 Committee of the Hospital General Universitario de Elche, Spain. All patients had been
286 diagnosed with GBM grade IV, and all of them exhibited an *IDH1* plus *IDH2* wild-type
287 genotype. Normal human brain RNA (frontal lobe; pool from 5 donors) was purchased
288 from BioChain and used as a control for gene expression experiments. A total of
289 12,516 genes were used to generate a custom Agilent Two-Color 8 x 15 K Agilent gene
290 expression DNA microarray, which were deposited in the NCBI Gene Expression
291 Omnibus (GEO) Database under accession number GSE182697 (28).

292 **Bioinformatics analysis**

293 The level of expression of human homologs of *Drosophila* ACD regulators was assessed
294 in seven different GBM patients versus control samples of the custom-made
295 microarray (GSE182697) (28). Statistical analysis of microarray data was done in
296 Multiexperiment Viewer (MeV) (58). Hierarchical clustering analyses were done
297 optimizing gene and sample leaf order and using Pearson Correlation for the distance
298 metric selection. Average linkage clustering was used as a linkage method. For the

299 Gene Distance Matrix (GDM), the distance, inverse of similarity, between two genes
300 was calculated using a distance metric as indicated in MeV.

301 **Human samples and cell lines**

302 Glioma samples were obtained with patients' written informed consent, in accordance
303 with the Declaration of Helsinki, and approved by the Ethics Committee at Hospital 12
304 de Octubre, Madrid, Spain (CEI 14/023). The primary glioblastoma cell lines were
305 provided by the Biobank at "Hospital 12 de Octubre". Fresh tissue samples were
306 enzymatically dissociated using Accumax (Millipore) and cultured in stem cell medium
307 (Neurobasal, Invitrogen), supplemented with N2 (1:100, Invitrogen), GlutaMAX (1:100,
308 Invitrogen), penicillin-streptomycin (1:100, Lonza), 0.4% heparin (Sigma-Aldrich), 40
309 ng/ml EGF and 20 ng/ml bFGF2 (Peprotech). The GB cell lines used in this study were:
310 GB4, GB5, GB7, GB18, GB19, 12o89, Astros (59,60) and HEK293T. The cell lines
311 HEK293T and Astros were maintained in Dulbecco´s modified Eagle Medium
312 supplemented with 10% fetal bovine serum 2 mM L-glutamine, 0.1% penicillin (100
313 U/ml) and streptomycin (100 µg/ml) and Non-Essential Aminoacids (NEA 1x).
314

315 <u>GBM-derived neurosphere cell cultures</u>

316 For stem cell culture of GBM-derived neuroespheres we used DMEM:F12 with FGF-2
317 (20 ng/ml), EGF-2 (20 ng/ml), and N2 supplements, 0.1% penicillin (100 U/ml) and
318 streptomycin (100 µg/ml), as previously described (61,62). The tumor spheres were
319 dissociated to single cells using Accumax, and $1x10^5$ dissociated cells/ml were plated in
320 a Flask and cultured for 6-7 days.
321

322 **In Silico Analysis**

323 Data from The Cancer Genome Atlas (TCGA) and the Chinese Glioma Genome Atlas
324 (CGGA) for GBM cohorts were accessed through UCSC Xena-Browser
325 (https://xenabrowser.net), and Gliovis (http://gliovis.bioinfo.cnio.es) for extraction of
326 overall survival data, gene expression levels, and distribution of genetic alterations.
327 Kaplan-Meier survival curves were generated by stratifying samples into low- and high-
328 expression groups for each gene. Survival differences between these groups were
329 assessed using the log-rank test.

330

331 **DNA Constructs and Lentiviral Production**

332 Lentiviral vectors were used to produce cells overexpressing *RAP2A* (*pLJM1RAP2A*
333 #Plasmid 19311, Addgene) or eGFP (pLJMEGFP #Plasmid 19319, Addgene) as infection
334 control. Infected cells were selected with Puromycin. To obtain the lentivirus, HEK293T
335 cells were transiently co-transfected with 5 µg of the appropriate lentiviral plasmid
336 (pLJEGFP or pLJRRap2A, respectively), 5 µg of the packaging plasmid pCMVdR8.74
337 (#Plasmid 22036, Addgene), and 5 µg of VERSUSV-G envelope protein plasmid pMD2G
338 (#Plasmid 12259, Addgene), using Lipofectamine Plus reagent (Invitrogen, Carisbad,
339 CA, USA). Lentiviral supernatants were collected after 48 h of HEK293T transfection.

340

341 **Neurosphere Immunofluorescences and Imaging**

342 For immunostaining, floating cultured neurospheres were incubated on Matrigel
343 coated micro slide glass for 2 hours at 37°C. After having been washed, the attached
344 neurospheres were fixed in 4% paraformaldehyde for 20 min. Cells were blocked for 1
345 h in 1% FBS and 0.1% Triton X-100 in PBS; then, they were incubated for 2 hours with

346 the primary antibody: mouse anti-CD133 (HB#7, Developmental Studies Hybridoma
347 Bank), mouse anti-Ki67 (3E6, Developmental Studies Hybridoma Bank), rabbit anti-
348 Sox2 (N1C3, GTX101507 GeneTex), mouse anti-Nestin (10c2, sc-23927, Santa Cruz
349 Biotechnology) and mouse anti-Numb (48, sc-136554, Santa Cruz Biotechnology). The
350 secondary antibodies used were Alexa555 goat anti-rabbit (A32732, Invitrogen) or
351 Alexa555 goat anti-mouse (A32727, Invitrogen). Phalloidin 633 (Sigma-Aldrich, 68825
352 Phalloidin-Atto 633) was added and incubated for 20 min in PBS; Vectashield Mounting
353 medium with DAPI (Linaris, H-1200) was added before mounting. Fluorescent images
354 were captured using a Super-resolution Inverted Confocal Microscope Zeiss LSM 880-
355 Airyscan Elyra PS.1. Images were analyzed using the image processing package FIJI
356 from ImageJ and assembled using Adobe Photoshop CS6 program.
357
358 Immunofluorescent quantification
359 Fluorescence intensity measurements were carried out using ImageJ software
360 package. In all cases, images of neuroespheres transfected with GFP (GB5, control) or
361 RAP2A (GB5-RAP2A) lentivirus were analyzed:
362 CD133: Using the "line tool", a line was drawn on the channel with the CD133 signal on
363 three different pictures per genotype. Fluorescence was measured across the line
364 sections with the "Plot Profile Tool", and reported as a subset of images showing the
365 signal intensity plot. For quantification, only the 100 highest gray value points, were
366 taken.
367 Sox: After adjusting the threshold on the channel with the Sox2 signal and eliminating
368 particles smaller than 5 microns, the fluorescence intensity was measured as the mean
369 gray value (sum of all pixels with gray values inside the selection, divided by the

370 number of pixels). In Figure 3 is shown one example out of three quantifications
371 achieved with at least 20 cells per genotype.
372 Nestin: The regions of interest (ROIs) were set with the "hand drawing tool" using the
373 Phalloidin staining to follow the cell periphery. At least 20 cells (ROIs) from three
374 different pictures were selected per condition. The background fluorescence was
375 subtracted from the mean gray value fluorescence for each well, and the fluorescence
376 intensity was normalized by the nuclear DAPI signal coming from the same cell (ROI).
377 Plot in Figure 3C represents the mean gray value that is the sum of all pixels with gray
378 values inside the selection divided by the number of pixels.
379
380 **RNA isolation and qRT-PCR assay**
381 Total RNA was extracted from 7 days old neurospheres using TRI reagent (AM9738,
382 Invitrogen) following manufacturer indications and quantified using a nanodrop (ND-
383 1000, Thermo Scientific). 2ug of RNA was treated with DNaseI (EN0521, Thermo
384 Scientific) and reverse transcribed with SuperScriptTM III Reverse Transcriptase
385 (1808044, Invitrogen). Quantitative real time PCR (qRT-PCR) was performed using
386 Power SYBR Green PCR Master Mix (PN4367218, Applied Biosystems), following
387 established protocols with 60°C for annealing/extension and 40 cycles of amplification
388 on a QuantStudioTM 3 apparatus (applied Biosystems). Act5 primers were used for
389 normalization, and relative expression was calculated using the comparative $\Delta\Delta$Ct. The
390 average of at least 3 independent experiments is shown in Figure 4.
391
392 **Neurosphere Western Blots**

393 Protein extracts were prepared by re-suspending cell pellets in a lysis buffer (50-mM
394 Tris, pH 7.5, 300-mM NaCl, 0.5% SDS, and 1% Triton X-100) and incubating the cells for
395 10 min at 95°C. The lysed extracts were centrifuged at 13,000 g for 10 min at room
396 temperature, and the protein concentration was determined using a commercially
397 available colorimetric assay (BCA Protein Assay Kit). Approximately 25 µg of protein
398 was resolved by 10% or 12,5% SDS-PAGE, and they were then transferred to a PVDF
399 membrane (Hybond-ECL, Amersham Biosciences). The membranes were blocked for
400 1 h at room temperature in TBS-T (10-mM Tris–HCl, pH 7.5, 100-mM NaCl, and 0.1%
401 Tween-20) with 5% skimmed milk, and then incubated overnight at 4°C with the
402 corresponding primary antibody diluted in TBS-T with 2,5% skimmed milk. After
403 washing 3 times with TBS-T, the membranes were incubated for 2 h at room
404 temperature with their corresponding secondary antibody, diluted in TBS-T with 2,5%
405 skimmed milk. The proteins were visible by enhanced chemiluminescence with ECL
406 (Pierce) using Amersham imager 680, and the signal was quantified by Fiji-ImageJ
407 software.
408
409 **Proliferative index (Ki67 analysis)**
410 The number of Ki67+ cells with respect to the total number of nuclei labelled with DAPI
411 within a given neurosphere were counted to calculate the Proliferative Index (PI),
412 which was expressed as the % of Ki67+ cells over total DAPI+ cells. More than 20
413 neurospheres coming from different pictures were analyzed.
414
415 **Sphere size measurement**

416 Glioblastoma cells (GB5 cell line) were infected by control lentivirus (LV-GFP) or by
417 lentivirus directing expression of *RAP2A* (LV-*RAP2A*). The tumor spheres were
418 Accumax-dissociated to single cells, during three consecutive passages. Seven days
419 after the third plating in a 6-well plate, spheres were captured using a 10x objective
420 (Carl Zeiss Axio Imager A1 microscope). 20 random pictures of each genotype were
421 taken and the images were analyzed by measuring the area of all the spheres present,
422 using the "freeform drawing tool" in the ImageJ software package. The data presented
423 show the average area measured in 3 independent experiments.
424
425 **Pair assay and Numb segregation analysis**
426 Dissociated cells were plated at low density on Matrigel-coated glass slides. Cultures
427 were incubated for 21 h at 37°C with 5% CO_2, fixed and immunolabeled for Numb, as
428 well as for DAPI to identify nuclei. First, isolated groups of cells (most probably coming
429 from the same single progenitor) were identified and the number of cells in each
430 cluster was annotated. For each identified DAPI-labeled pair, the localization of Numb
431 was visualized and scored from at least 100 cell pairs. Images in Figure 6 were acquired
432 in an Inverted Microscope Leica Thunder Imager.
433
434 **Statistical analysis**
435 The data were first analyzed using the Shapiro-Wilk test to determine whether the
436 sample followed a normal distribution. Parametric T-test or a nonparametric two-
437 tailed Mann Whitney U test for those that did not follow a normal distribution were
438 used to compare statistical differences between two different groups. Mean and
439 standard deviation values were calculated by standard methods. A Chi-square test was

used to analyze the data in Figure 2C. To assume statistical significance, *p*-values were determined below 0.05. Sample size (n) and the *p*-value are indicated in the figure or figure legend; * $p < 0.05$, ** $p < 0.01$, *** $p < 0.001$, ns: not significant ($p > 0.05$).

Acknowledgements: We thank the Bloomington *Drosophila* Stock Center at the University of Indiana and the Developmental Studies Hybridoma Bank at the University of Iowa for kindly providing fly strains and reagents. R.G. was funded by "Instituto de Salud Carlos III (ISCIII)" through the project "Miguel Servet Contracts" (CP21/00116), PI22/01171 and co-funded by the European Union. M.S. was supported by the Spanish grant from the Instituto de Salud Carlos III (ISCIII) PI22/00824. A.C. was financed by the Spanish grants from the Ministry of Science, Innovation and Universities (PGC2018-097093-B-100), the Ministry of Science and Innovation (PID2021-123196NB-100), the Generalitat Valenciana Prometeo/2021/052 grant and by FEDER (European Regional Development Fund). The "Instituto de Neurociencias" in Alicante is a "Severo Ochoa Center of Excellence in R&D". Our group belongs to "Conexión Cáncer- CSIC".

Author contributions: M.F. participated in the design of the experiments, conducted most of them and analyzed the data; R.G. developed the GB lines and performed the in silico analyses; V.M.B. and M.S. carried out the GB microarray and bioinformatics analysis; A.C. conceived the study and wrote the manuscript.

Conflict of interest: The authors declare no competing interests

464 **Figure legends**

465

466 **Figure 1.**

467 ***RAP2A* is highly downregulated in GBM patients**.

468 (**A, B)** Analysis of GBM patient versus control samples focused on the level of

469 expression of human homologs of *Drosophila* ACD regulators by Hierarchical clustering

470 (**A**) and the Gene Distance Matrix (**B**). Color-coded scale bar indicates fold level of

471 expression. **(C)** Kaplan-Meier survival curves corresponding to patients in the TCGA

472 (IDHwt) and Gravendeel (IDHwt) cohort in GBM datasets. Low *RAP2A* expression levels

473 in human GBM are associated with a poor prognosis.

474

475 **Figure 2**.

476 ***Drosophila RAP2A* homolog *Rap2l* regulates ACD.**

477 **(A)** *Drosophila* NBII lineage; the only NB per lineage expresses the transcription factor

478 Dpn, while mature INPs express both Dpn and Ase; iINP, immature INP; mINP, mature

479 INP; GMC, Ganglion Mother Cell. **(B)** Confocal micrographs showing a control larval

480 brain NBII lineage with one NB (Dpn^+ Ase^-) and an NBII lineage in which *Rap2l* has been

481 downregulated displaying an ectopic NB (eNB). **(C)** *Rap2l* downregulation in NBII

482 lineages by the *wor-Gal4 ase-Gal80* (an NBII-specific driver) causes Cno and Numb

483 localization failures (green arrows) in dividing progenitors (NB or INPs), while aPKC

484 localization is not significantly altered (red arrows). Data shown in the scaled bar

485 graphs was analyzed with a Chi-square test, $*p<0.05$, $**p<0.01$, ns, not significant,

486 n=number of NB lineages analyzed (in B) or number of dividing cells analyzed (in C);

487 scale bar: 10 μm.

488 **Figure 3.**

489 ***RAP2A* expression in GBM neurosphere cultures reduces the stem cell population.**

490 **(A)** Different GBM cell lines show similar *RAP2A* mRNA levels and significantly lower
491 levels than in control Astros. **(B)** *RAP2A* mRNA levels are significantly higher in the GB5
492 line after infecting this line with *RAP2A* (GB5-RAP2A). Data shown in the scaled bar
493 graphs in A and B was analyzed with an ANOVA and a T-test, respectively; error bars
494 show the SD; n= 2 (in A) and 3 (in B) different experiments. **(C)** Immunofluorescences
495 of the GSC stem cell markers CD133, SOX2 and Nestin reveal a significant reduction in
496 the protein intensity in the GB5 RAP2A-expressing neurospheres (GB5-RAP2A)
497 compared to the control neurospheres (GB5). Data shown in the box plots was
498 analyzed with a U Mann-Whitney for CD133 and Nestin and with a T-test for Sox; the
499 central lines represent the median and the box limits the lower and upper quartiles, as
500 determined by R software; crosses represent sample means; error bars indicate the
501 SEM; n= number of sample points; *p* values: **p*<0.05, ***p*<0.01, ****p*<0.001, ns, not
502 significant; scale bar: 10 μm.

503

504 **Figure 4.**

505 ***RAP2A* expression in GBM neurosphere cultures reduces the stem cell population.**
506 RT-PCRs and Westerns blots show a significant decrease in the mRNA and protein
507 expression levels, respectively, of the GSC markers CD133, SOX2 and Nestin in the GB5
508 RAP2A-expressing neurospheres (GB5-RAP2A) compared to the control neurospheres
509 (GB5). Data shown in the scaled bar graphs was analyzed with an unpaired two-tailed
510 Student´s *t* test; error bars show the SD; n= 3 different experiments; *p* values: **p*<0.05,
511 ***p*<0.01.

512 **Figure 5.**

513 ***RAP2A* expression in GBM neurosphere cultures decreases cell proliferation and**

514 **sphere size.**

515 **(A)** GB5 neurospheres expressing RAP2A (GB5-RAP2A) show a significantly lower

516 number of Ki67 expressing cells per neurosphere than control GB5 neurospheres. Data

517 shown in the box plots was analyzed with a T-test; the central lines represent the

518 median and the box limits the lower and upper quartiles, as determined by R software;

519 crosses represent sample means; error bars indicate the SEM; n= number of sample

520 points. **(B)** GB5 neurospheres expressing RAP2A (GB5-RAP2A) show a significant

521 decrease in their size compared to control GB5 neurospheres of the same stage. Data

522 shown in the scaled bar graphs was analyzed with an unpaired two-tailed Student´s T-

523 test; error bars show the SD; n= total number of neurospheres of 3 different

524 experiments; *p* values: *$p<0.05$; scale bars: 10 μm (in A) and 100μm (in B).

525

526 **Figure 6.**

527 ***RAP2A* expression in GBM neurosphere cultures fosters ACD in GSCs.**

528 **(A)** Early stage GB5 neurospheres expressing RAP2A (GB5-RAP2A) show an odd

529 number of cells significantly more frequently than control GB5 neurospheres, which

530 show more frequently an even number of cells. **(B)** GB5-RAP2A dividing cells show a

531 significant increase in the number of asymmetric NUMB localization in the progeny,

532 compared to control GB5 dividing cells. Data shown in the bar graphs was analyzed

533 with a Chi-Square test with Yates correction; n= number of neurosphere cell clusters

534 analyzed. *p* values: **$p<0.01$; scale bar: 20 μm.

535

536 **References**

537 1. Knoblich JA. Mechanisms of asymmetric stem cell division. Cell **2008**;132:583-
538 97
539 2. Knoblich JA. Asymmetric cell division: recent developments and their
540 implications for tumour biology. Nat Rev Mol Cell Biol **2010**;11:849-60
541 3. Caussinus E, Gonzalez C. Induction of tumor growth by altered stem-cell
542 asymmetric division in Drosophila melanogaster. Nat Genet **2005**;37:1125-9
543 4. Gateff E. Malignant neoplasms of genetic origin in Drosophila melanogaster.
544 Science **1978**;200:1448-59
545 5. Albertson R, Doe CQ. Dlg, Scrib and Lgl regulate neuroblast cell size and mitotic
546 spindle asymmetry. Nat Cell Biol **2003**;5:166-70
547 6. Bello B, Reichert H, Hirth F. The brain tumor gene negatively regulates neural
548 progenitor cell proliferation in the larval central brain of Drosophila.
549 Development **2006**;133:2639-48
550 7. Betschinger J, Mechtler K, Knoblich JA. Asymmetric segregation of the tumor
551 suppressor brat regulates self-renewal in Drosophila neural stem cells. Cell
552 **2006**;124:1241-53
553 8. Bowman SK, Rolland V, Betschinger J, Kinsey KA, Emery G, Knoblich JA. The
554 tumor suppressors Brat and Numb regulate transit-amplifying neuroblast
555 lineages in Drosophila. Dev Cell **2008**;14:535-46
556 9. Ohshiro T, Yagami T, Zhang C, Matsuzaki F. Role of cortical tumour-suppressor
557 proteins in asymmetric division of Drosophila neuroblast. Nature
558 **2000**;408:593-6
559 10. Peng CY, Manning L, Albertson R, Doe CQ. The tumour-suppressor genes lgl and
560 dlg regulate basal protein targeting in Drosophila neuroblasts. Nature
561 **2000**;408:596-600
562 11. Lee CY, Wilkinson BD, Siegrist SE, Wharton RP, Doe CQ. Brat is a Miranda cargo
563 protein that promotes neuronal differentiation and inhibits neuroblast self-
564 renewal. Dev Cell **2006**;10:441-9
565 12. Bonnet D, Dick JE. Human acute myeloid leukemia is organized as a hierarchy
566 that originates from a primitive hematopoietic cell. Nat Med **1997**;3:730-7
567 13. Lapidot T, Sirard C, Vormoor J, Murdoch B, Hoang T, Caceres-Cortes J*, et al.* A
568 cell initiating human acute myeloid leukaemia after transplantation into SCID
569 mice. Nature **1994**;367:645-8
570 14. Bajaj J, Diaz E, Reya T. Stem cells in cancer initiation and progression. J Cell Biol
571 **2020**;219
572 15. Reya T, Morrison SJ, Clarke MF, Weissman IL. Stem cells, cancer, and cancer
573 stem cells. Nature **2001**;414:105-11
574 16. Moore N, Lyle S. Quiescent, slow-cycling stem cell populations in cancer: a
575 review of the evidence and discussion of significance. J Oncol **2011**;2011
576 17. Rosen JM, Jordan CT. The increasing complexity of the cancer stem cell
577 paradigm. Science **2009**;324:1670-3
578 18. Yadav UP, Singh T, Kumar P, Sharma P, Kaur H, Sharma S*, et al.* Metabolic
579 Adaptations in Cancer Stem Cells. Front Oncol **2020**;10:1010
580 19. Bajaj J, Zimdahl B, Reya T. Fearful symmetry: subversion of asymmetric division
581 in cancer development and progression. Cancer Res **2015**;75:792-7

582 20. Chao S, Yan H, Bu P. Asymmetric division of stem cells and its cancer relevance.
583 Cell Regen **2024**;13:5
584 21. Galli R, Binda E, Orfanelli U, Cipelletti B, Gritti A, De Vitis S*, et al.* Isolation and
585 characterization of tumorigenic, stem-like neural precursors from human
586 glioblastoma. Cancer Res **2004**;64:7011-21
587 22. Singh SK, Clarke ID, Terasaki M, Bonn VE, Hawkins C, Squire J*, et al.*
588 Identification of a cancer stem cell in human brain tumors. Cancer Res
589 **2003**;63:5821-8
590 23. Singh SK, Hawkins C, Clarke ID, Squire JA, Bayani J, Hide T*, et al.* Identification of
591 human brain tumour initiating cells. Nature **2004**;432:396-401
592 24. Biserova K, Jakovlevs A, Uljanovs R, Strumfa I. Cancer Stem Cells: Significance in
593 Origin, Pathogenesis and Treatment of Glioblastoma. Cells **2021**;10
594 25. Chen J, Li Y, Yu TS, McKay RM, Burns DK, Kernie SG*, et al.* A restricted cell
595 population propagates glioblastoma growth after chemotherapy. Nature
596 **2012**;488:522-6
597 26. Hassn Mesrati M, Behrooz AB, Y Abuhamad A, Syahir A. Understanding
598 Glioblastoma Biomarkers: Knocking a Mountain with a Hammer. Cells **2020**;9
599 27. Tang X, Zuo C, Fang P, Liu G, Qiu Y, Huang Y*, et al.* Targeting Glioblastoma Stem
600 Cells: A Review on Biomarkers, Signal Pathways and Targeted Therapy. Front
601 Oncol **2021**;11:701291
602 28. Larriba E, de Juan Romero C, García-Martínez A, Quintanar T, Rodríguez-
603 Lescure Á, Soto JL*, et al.* Identification of new targets for glioblastoma therapy
604 based on a DNA expression microarray. Comput Biol Med **2024**;179:108833
605 29. Chen G, Kong J, Tucker-Burden C, Anand M, Rong Y, Rahman F*, et al.* Human
606 Brat ortholog TRIM3 is a tumor suppressor that regulates asymmetric cell
607 division in glioblastoma. Cancer Res **2014**;74:4536-48
608 30. Wang L, Zhan W, Xie S, Hu J, Shi Q, Zhou X*, et al.* Over-expression of Rap2a
609 inhibits glioma migration and invasion by down-regulating p-AKT. Cell Biol Int
610 **2014**;38:326-34
611 31. Wang L, Zhu B, Wang S, Wu Y, Zhan W, Xie S*, et al.* Regulation of glioma
612 migration and invasion via modification of Rap2a activity by the ubiquitin ligase
613 Nedd4-1. Oncol Rep **2017**;37:2565-74
614 32. Carmena A, Makarova A, Speicher S. The Rap1-Rgl-Ral signaling network
615 regulates neuroblast cortical polarity and spindle orientation. J Cell Biol
616 **2011**;195:553-62
617 33. Bello BC, Izergina N, Caussinus E, Reichert H. Amplification of neural stem cell
618 proliferation by intermediate progenitor cells in Drosophila brain development.
619 Neural Dev **2008**;3:5
620 34. Boone JQ, Doe CQ. Identification of Drosophila type II neuroblast lineages
621 containing transit amplifying ganglion mother cells. Dev Neurobiol
622 **2008**;68:1185-95
623 35. Wodarz A, Ramrath A, Grimm A, Knust E. Drosophila atypical protein kinase C
624 associates with Bazooka and controls polarity of epithelia and neuroblasts. J
625 Cell Biol **2000**;150:1361-74
626 36. Knoblich JA, Jan LY, Jan YN. Asymmetric segregation of Numb and Prospero
627 during cell division. Nature **1995**;377:624-7

628 37. Speicher S, Fischer A, Knoblich J, Carmena A. The PDZ protein Canoe regulates
629 the asymmetric division of Drosophila neuroblasts and muscle progenitors. Curr
630 Biol **2008**;18:831-7
631 38. Gerdes J, Schwab U, Lemke H, Stein H. Production of a mouse monoclonal
632 antibody reactive with a human nuclear antigen associated with cell
633 proliferation. Int J Cancer **1983**;31:13-20
634 39. Sun X, Kaufman PD. Ki-67: more than a proliferation marker. Chromosoma
635 **2018**;127:175-86
636 40. Yan B. Numb--from flies to humans. Brain Dev **2010**;32:293-8
637 41. Morrison SJ, Kimble J. Asymmetric and symmetric stem-cell divisions in
638 development and cancer. Nature **2006**;441:1068-74
639 42. Cayouette M, Raff M. Asymmetric segregation of Numb: a mechanism for
640 neural specification from Drosophila to mammals. Nat Neurosci **2002**;5:1265-9
641 43. Cicalese A, Bonizzi G, Pasi CE, Faretta M, Ronzoni S, Giulini B*, et al.* The tumor
642 suppressor p53 regulates polarity of self-renewing divisions in mammary stem
643 cells. Cell **2009**;138:1083-95
644 44. Ortega-Campos SM, García-Heredia JM. The Multitasker Protein: A Look at the
645 Multiple Capabilities of NUMB. Cells **2023**;12
646 45. Li Z, Zhang YY, Zhang H, Yang J, Chen Y, Lu H. Asymmetric Cell Division and
647 Tumor Heterogeneity. Front Cell Dev Biol **2022**;10:938685
648 46. Dey-Guha I, Wolfer A, Yeh AC, G Albeck J, Darp R, Leon E*, et al.* Asymmetric
649 cancer cell division regulated by AKT. Proc Natl Acad Sci U S A **2011**;108:12845-
650 50
651 47. Sugiarto S, Persson AI, Munoz EG, Waldhuber M, Lamagna C, Andor N*, et al.*
652 Asymmetry-defective oligodendrocyte progenitors are glioma precursors.
653 Cancer Cell **2011**;20:328-40
654 48. Daynac M, Chouchane M, Collins HY, Murphy NE, Andor N, Niu J*, et al.* Lgl1
655 controls NG2 endocytic pathway to regulate oligodendrocyte differentiation
656 and asymmetric cell division and gliomagenesis. Nat Commun **2018**;9:2862
657 49. Bu P, Chen KY, Chen JH, Wang L, Walters J, Shin YJ*, et al.* A microRNA miR-34a-
658 regulated bimodal switch targets Notch in colon cancer stem cells. Cell Stem
659 Cell **2013**;12:602-15
660 50. Hwang WL, Jiang JK, Yang SH, Huang TS, Lan HY, Teng HW*, et al.* MicroRNA-
661 146a directs the symmetric division of Snail-dominant colorectal cancer stem
662 cells. Nat Cell Biol **2014**;16:268-80
663 51. Homem CC, Knoblich JA. Drosophila neuroblasts: a model for stem cell biology.
664 Development **2012**;139:4297-310
665 52. Samanta P, Bhowmik A, Biswas S, Sarkar R, Ghosh R, Pakhira S*, et al.*
666 Therapeutic Effectiveness of Anticancer Agents Targeting Different Signaling
667 Molecules Involved in Asymmetric Division of Cancer Stem Cell. Stem Cell Rev
668 Rep **2023**;19:1283-306
669 53. Chao S, Zhang F, Yan H, Wang L, Zhang L, Wang Z*, et al.* Targeting intratumor
670 heterogeneity suppresses colorectal cancer chemoresistance and metastasis.
671 EMBO Rep **2023**;24:e56416
672 54. Hitomi M, Chumakova AP, Silver DJ, Knudsen AM, Pontius WD, Murphy S*, et al.*
673 Asymmetric cell division promotes therapeutic resistance in glioblastoma stem
674 cells. JCI Insight **2021**;6

675 55. de Thé H. Differentiation therapy revisited. Nat Rev Cancer **2018**;18:117-27
676 56. Neumuller RA, Richter C, Fischer A, Novatchkova M, Neumuller KG, Knoblich JA.
677 Genome-wide analysis of self-renewal in Drosophila neural stem cells by
678 transgenic RNAi. Cell Stem Cell **2011**;8:580-93
679 57. Rives-Quinto N, Franco M, de Torres-Jurado A, Carmena A. Synergism between
680 canoe and scribble mutations causes tumor-like overgrowth via Ras activation
681 in neural stem cells and epithelia. Development **2017**;144:2570-83
682 58. Saeed AI, Sharov V, White J, Li J, Liang W, Bhagabati N*, et al.* TM4: a free, open-
683 source system for microarray data management and analysis. Biotechniques
684 **2003**;34:374-8
685 59. Gargini R, Escoll M, García E, García-Escudero R, Wandosell F, Antón IM. WIP
686 Drives Tumor Progression through YAP/TAZ-Dependent Autonomous Cell
687 Growth. Cell Rep **2016**;17:1962-77
688 60. Gargini R, Segura-Collar B, Herránz B, García-Escudero V, Romero-Bravo A,
689 Núñez FJ*, et al.* The IDH-TAU-EGFR triad defines the neovascular landscape of
690 diffuse gliomas. Sci Transl Med **2020**;12
691 61. Ponti D, Costa A, Zaffaroni N, Pratesi G, Petrangolini G, Coradini D*, et al.*
692 Isolation and in vitro propagation of tumorigenic breast cancer cells with
693 stem/progenitor cell properties. Cancer Res **2005**;65:5506-11
694 62. Gargini R, Cerliani JP, Escoll M, Antón IM, Wandosell F. Cancer stem cell-like
695 phenotype and survival are coordinately regulated by Akt/FoxO/Bim pathway.
696 Stem Cells **2015**;33:646-60
697

Figure 1

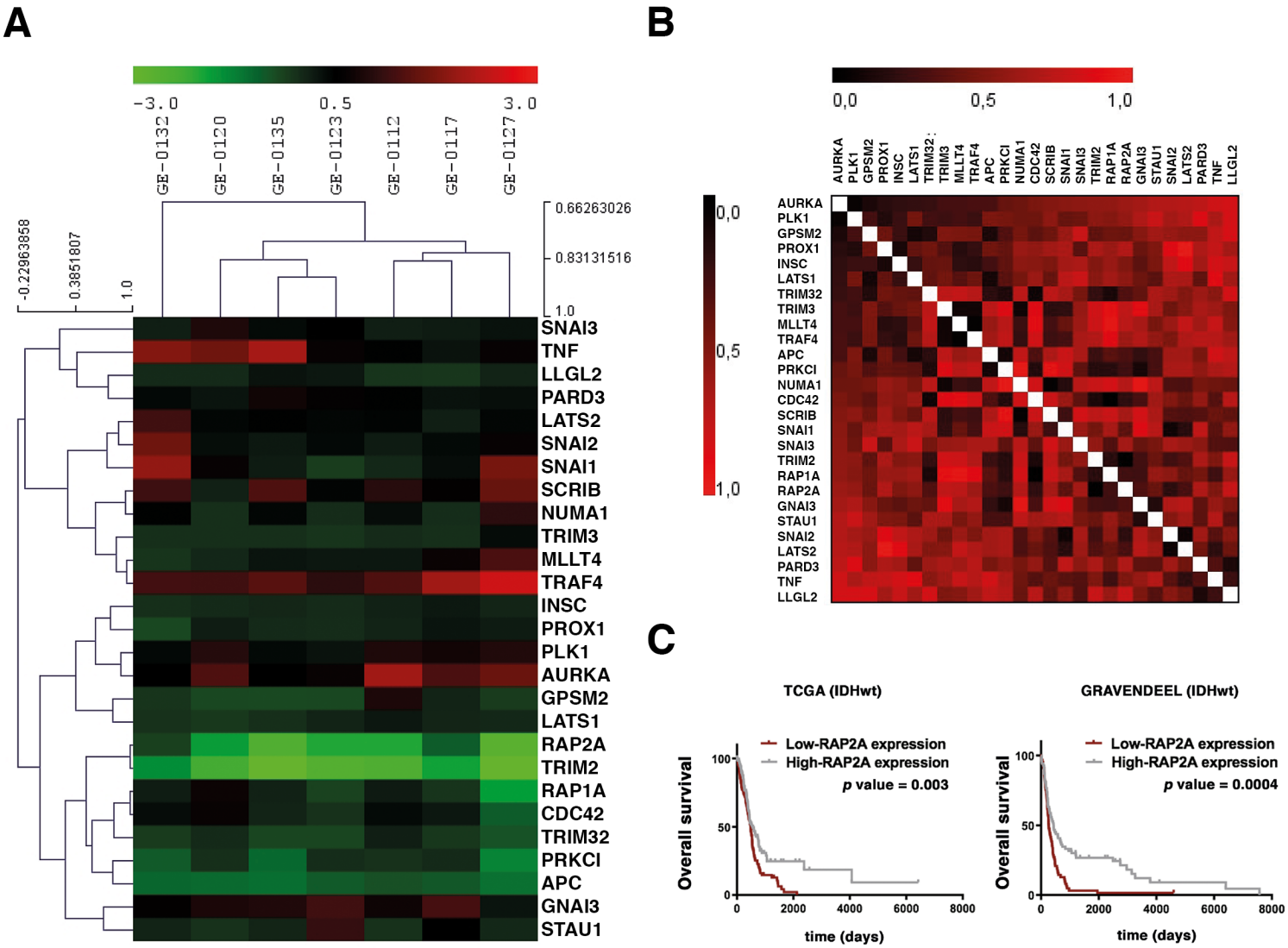
A
-3.0
0.5
3.0
GE-0132
GE-0120
GE-0135
GE-0123
GE-0112
GE-0117
GE-0127
-0.22963858
0.3851807
1.0
0.66263026
0.83131516
1.0
SNAI3
TNF
LLGL2
PARD3
LATS2
SNAI2
SNAI1
SCRIB
NUMA1
TRIM3
MLLT4
TRAF4
INSC
PROX1
PLK1
AURKA
GPSM2
LATS1
RAP2A
TRIM2
RAP1A
CDC42
TRIM32
PRKCI
APC
GNAI3
STAU1
B
0,0
0,5
1,0
AURKA
PLK1
GPSM2
PROX1
INSC
LATS1
TRIM32
TRIM3
MLLT4
TRAF4
APC
PRKCI
NUMA1
CDC42
SCRIB
SNAI1
SNAI3
TRIM2
RAP1A
RAP2A
GNAI3
STAU1
SNAI2
LATS2
PARD3
TNF
LLGL2
C
TCGA (IDHwt)
Low-RAP2A expression
High-RAP2A expression
p value = 0.003
Overall survival
time (days)
GRAVENDEEL (IDHwt)
Low-RAP2A expression
High-RAP2A expression
p value = 0.0004
Overall survival
time (days)

Figure 2

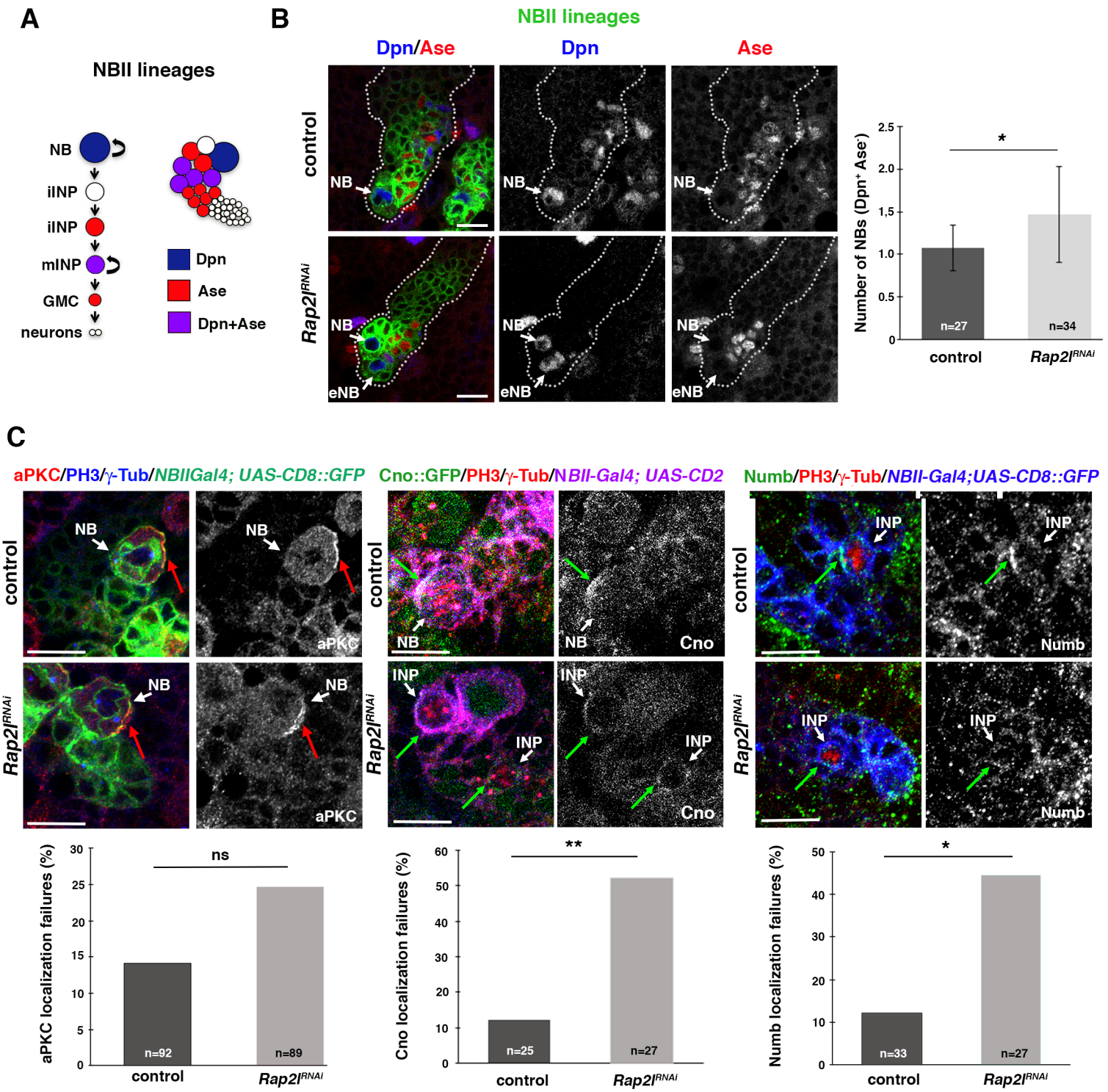
A
NBII lineages
NB
iINP
iINP
mINP
GMC
neurons
Dpn
Ase
Dpn+Ase
B
NBII lineages
Dpn/Ase
Dpn
Ase
control
Rap2l RNAi
NB
eNB
Number of NBs (Dpn+ Ase-)
n=27
n=34
control
Rap2l RNAi
C
aPKC/PH3/γ-Tub/NBIIGal4; UAS-CD8::GFP
Cno::GFP/PH3/γ-Tub/NBII-Gal4; UAS-CD2
Numb/PH3/γ-Tub/NBII-Gal4;UAS-CD8::GFP
aPKC
Cno
Numb
INP
aPKC localization failures (%)
ns
n=92
n=89
Cno localization failures (%)
**
n=25
n=27
Numb localization failures (%)
*
n=33
n=27

Figure 3

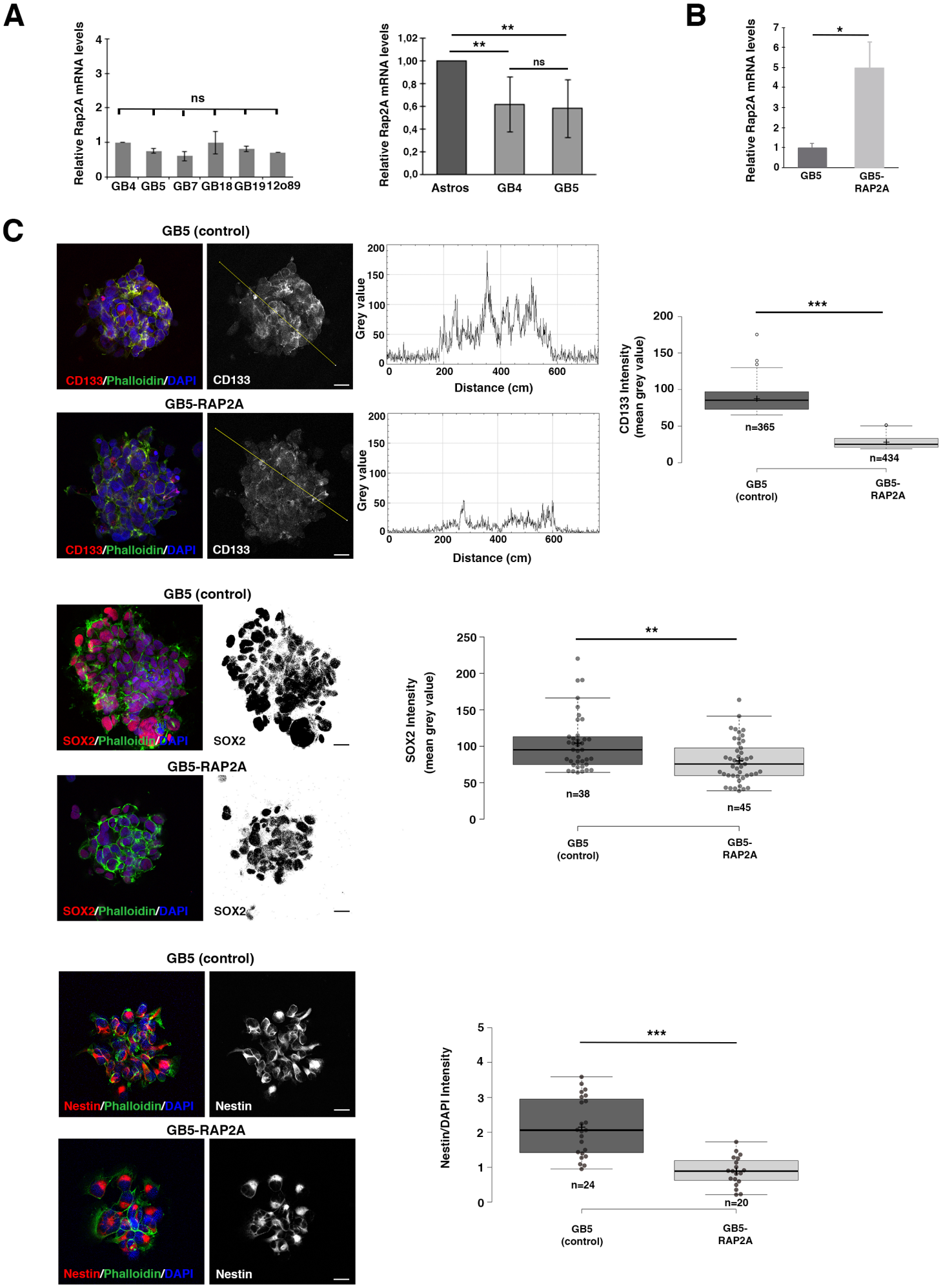
A
Relative Rap2A mRNA levels
ns
GB4 GB5 GB7 GB18 GB19 12o89
Relative Rap2A mRNA levels
**
**
ns
Astros GB4 GB5
B
Relative Rap2A mRNA levels
*
GB5 GB5-RAP2A
C
GB5 (control)
CD133/Phalloidin/DAPI
CD133
Grey value
Distance (cm)
GB5-RAP2A
CD133/Phalloidin/DAPI
CD133
Grey value
Distance (cm)
CD133 Intensity (mean grey value)
***
n=365
n=434
GB5 (control)
GB5-RAP2A
GB5 (control)
SOX2/Phalloidin/DAPI
SOX2
GB5-RAP2A
SOX2/Phalloidin/DAPI
SOX2
SOX2 Intensity (mean grey value)
**
n=38
n=45
GB5 (control)
GB5-RAP2A
GB5 (control)
Nestin/Phalloidin/DAPI
Nestin
GB5-RAP2A
Nestin/Phalloidin/DAPI
Nestin
Nestin/DAPI Intensity
***
n=24
n=20
GB5 (control)
GB5-RAP2A

Figure 4

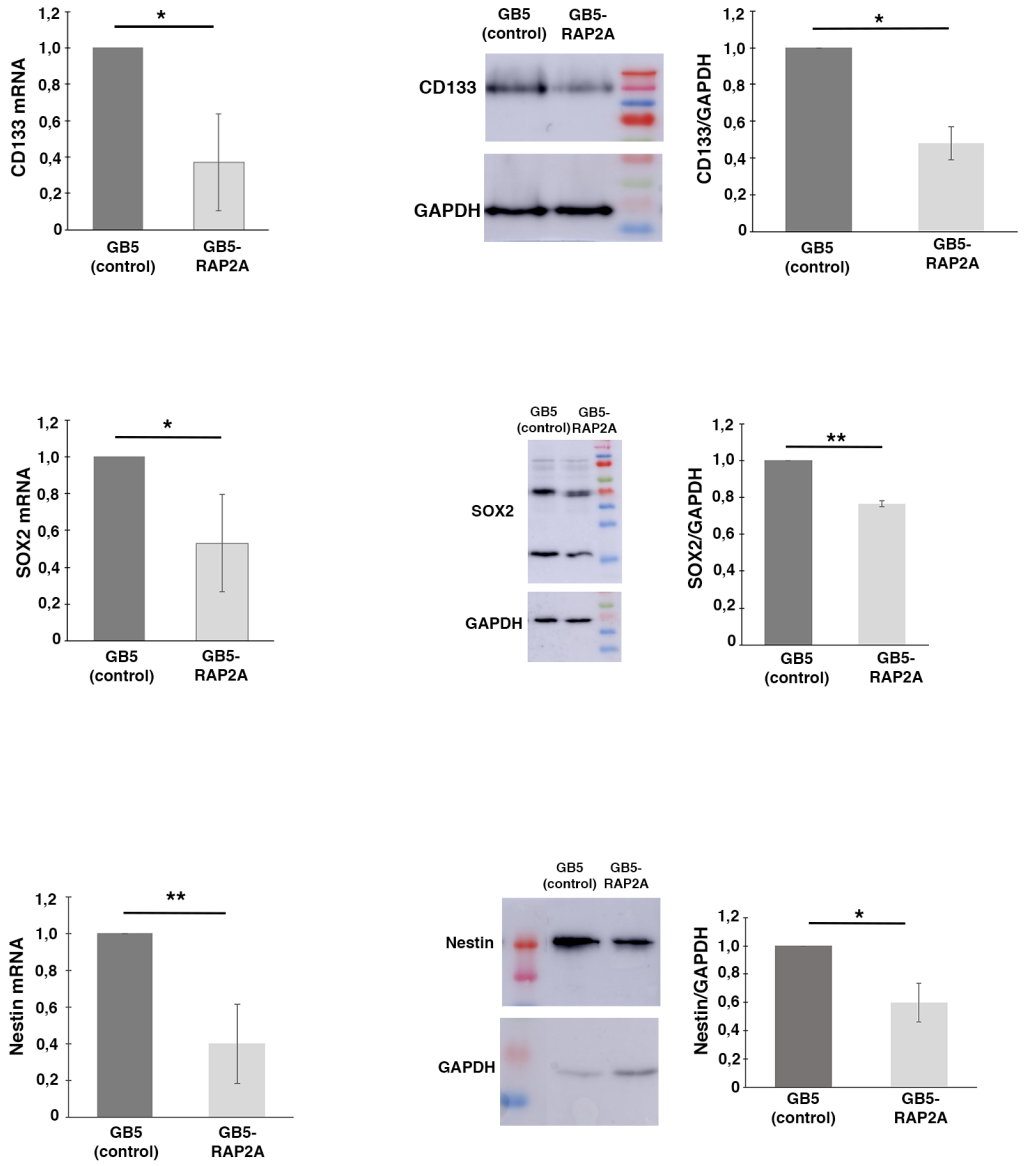
CD133 mRNA
1,2
1,0
0,8
0,6
0,4
0,2
0
*
GB5 (control)
GB5-RAP2A
GB5 (control)
GB5-RAP2A
CD133
GAPDH
CD133/GAPDH
*
SOX2 mRNA
*
SOX2
GAPDH
SOX2/GAPDH
**
Nestin mRNA
**
Nestin
GAPDH
Nestin/GAPDH
*

Figure 5

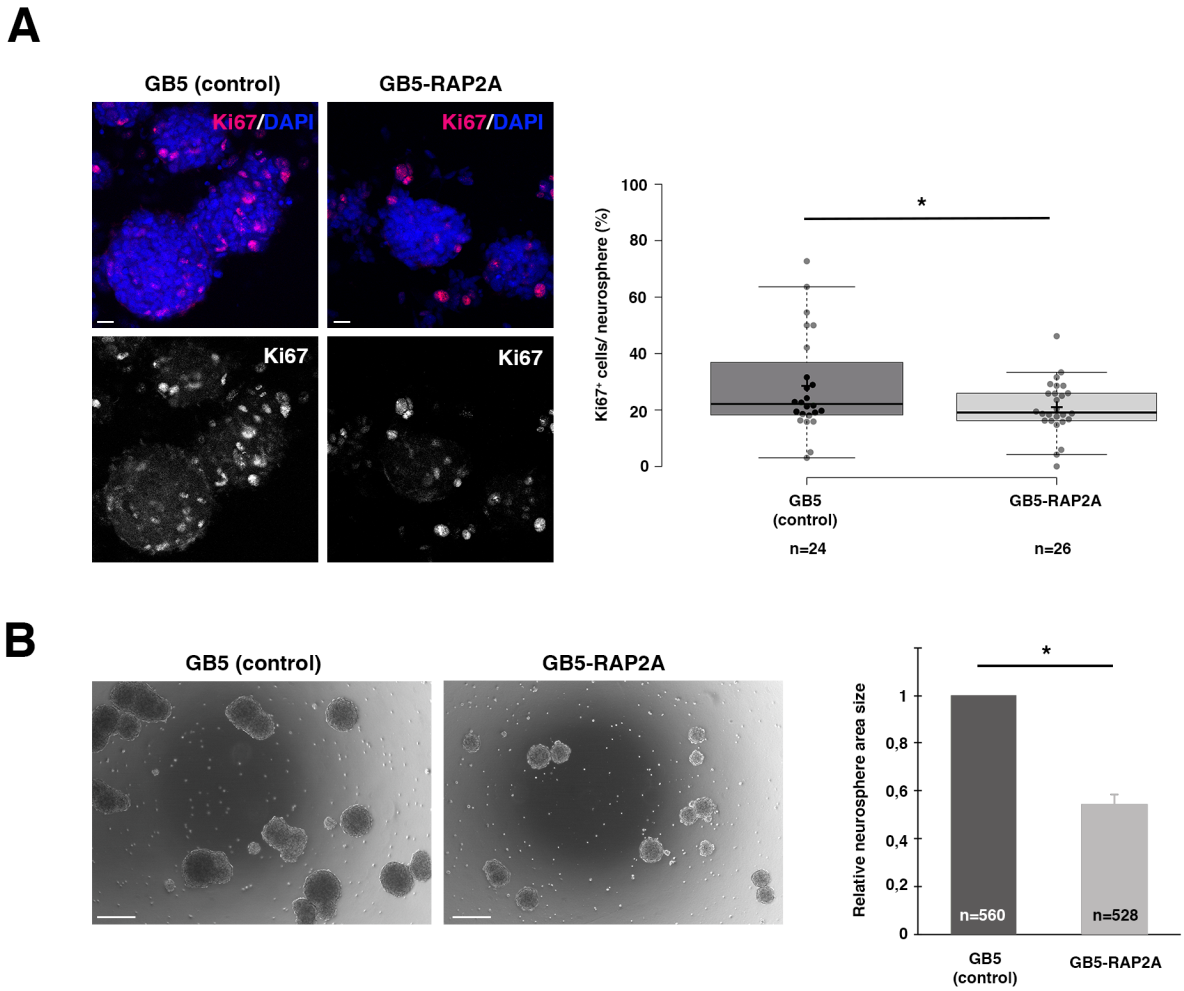
A
GB5 (control)
GB5-RAP2A
Ki67/DAPI
Ki67/DAPI
Ki67
Ki67
KI67+ cells/ neurosphere (%)
100
80
60
40
20
0
*
GB5
(control)
GB5-RAP2A
n=24
n=26
B
GB5 (control)
GB5-RAP2A
Relative neurosphere area size
1
0,8
0,6
0,4
0,2
0
*
n=560
n=528
GB5
(control)
GB5-RAP2A

Figure 6

A

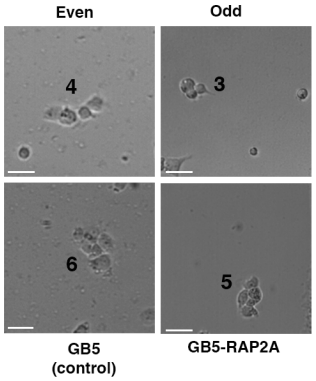
Even
Odd
4
3
6
5
GB5
(control)
GB5-RAP2A

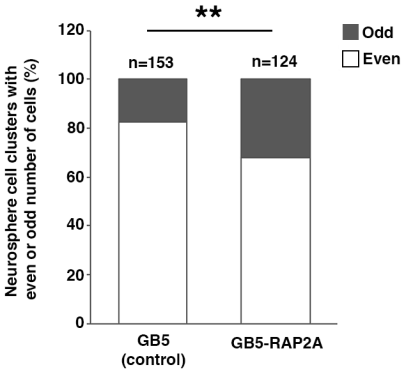
**
Odd
Even
n=153
n=124
Neurosphere cell clusters with even or odd number of cells (%)
120
100
80
60
40
20
0
GB5
(control)
GB5-RAP2A

B

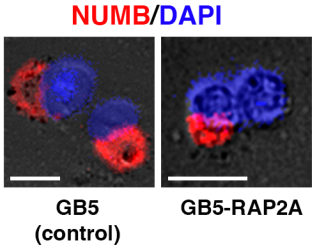
NUMB/DAPI
GB5
(control)
GB5-RAP2A

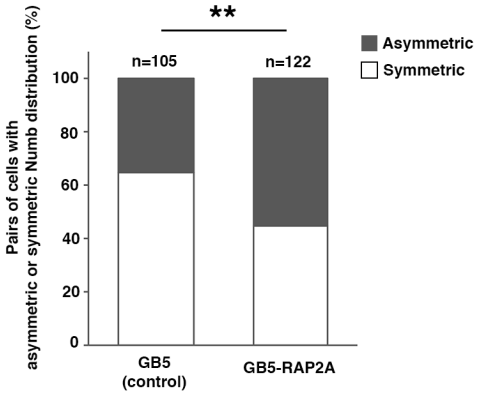
**
Asymmetric
Symmetric
n=105
n=122
Pairs of cells with asymmetric or symmetric Numb distribution (%)
100
80
60
40
20
0
GB5
(control)
GB5-RAP2A